ISSN 1990-7931, Russian Journal of Physical Chemistry B, 2025, Vol. 19, No. 1, pp. 200–216. © Pleiades Publishing, Ltd., 2025.

CHEMICAL PHYSICS OF NANOMATERIALS

Evaluation of Molecular Structure and Physico-chemical Properties of Boron Nitride Nanomaterial for Capturing Transition Metals (Chromium, Manganese, Iron, Zinc, Tungsten or Cadmium): a Theoretical Study

F. Mollaamin[a], * and M. Monajjemi[b]

[a] *Department of Biomedical Engineering, Faculty of Engineering and Architecture, Kastamonu University, Kastamonu, Turkey*
[b] *Department of Chemical Engineering, Central Tehran Branch, Islamic Azad University, Tehran, Iran*
**e-mail: fmollaamin@kastamonu.edu.tr*

Received May 24, 2024; revised September 12, 2024; accepted September 20, 2024

Abstract—Soil pollution caused by potentially toxic transition metals has become a worldwide environmental issue. Geogenic processes and anthropogenic activities are two important sources of soil pollution. Soils may inherit toxic transition metals from parent materials; however, soil pollution mostly results from industrial and agricultural activities. Contamination by transition metals can be indicated by the changes in chemical, biochemical, and microbial properties of soils and plant responses. The target of this research is removing transition metals of chromium (Cr), manganese (Mn), iron (Fe), zinc (Zn), tungsten (W), cadmium (Cd) from soil due to nanomaterial-based boron nitride nanocage (B_5N_{10}-nc). The electromagnetic and thermodynamic attributes of toxic transition metals trapped in B_5N_{10}-nc was depicted by materials modeling. The encapsulation of these elements occurs via chemisorption. It has been studied the behavior of trapping of Cr, Mn, Fe, Zn, W, Cd by B_5N_{10}-nc for sensing the soil metal cations. B_5N_{10}-nc was designed in the existence of transition metals (Cr, Mn, Fe, Zn, W, Cd). Case characterization was performed by DFT method. The nature of covalent features for these complexes has represented the analogous energy amount and vision of the partial density of states between the *p* states of boron and nitrogen in B_5N_{10}-nc with *d* states of transition metals in X ↔ B_5N_{10}-nc complexes (X= Cr, Mn, Fe, Zn, W, Cd). Furthermore, the nuclear magnetic resonance (NMR) analysis indicated the notable peaks surrounding Cr, Mn, Fe, Zn, W, Cd through the trapping in the B_5N_{10}-nc during atom detection and removal from soil; however, it can be seen some fluctuations in the chemical shielding treatment of isotropic and anisotropy tensors. Based on the results in this research, the selectivity of toxic metal, metalloid and nonmetal elements adsorption by B_5N_{10}-nc (atom sensor) have been indicated as: Cd > Zn > Fe > Cr > Mn ≈ W. In this article, it is proposed that toxic metal, metalloid and nonmetal elements–adsorbed might be applied to design and expand the optoelectronic specifications of B_5N_{10}-nc for generating photoelectric instruments toward soil purification.

Keywords: soil contamination, B_5N_{10}-nc, molecular modeling, nanomaterial, DFT
DOI: 10.1134/S1990793124701665

1. INTRODUCTION

Geogenic processes and anthropogenic activities are two important sources of soil pollution. Soils may inherit toxic metals from parent materials; however, soil pollution mostly results from industrial and agricultural activities [1–8]. Contamination by metals can be indicated by the changes in chemical, biochemical, and microbial properties of soils and plant responses [9–11]. The total concentration of toxic metals in soil is still the most widely used indicator for risk assessment although extractable amounts have been reported to be more closely related to plant uptake [12–16]. Heavy metals remark to some metals and metalloids having biological toxicity like Cd, Hg, As, Pb, and Cr [17]. Heavy metal contamination to soil and the environment has been accelerated in modern society due to industrialization, rapidly expanded world population, and intensified agriculture [18–20]. Accumulation of heavy metals often results in soil/water degradation and ecosystem malfunction. Moreover, heavy metals enter food chains from polluted soil, water, and air, and consequently cause food contamination, thus posing a threat to human and animal health [21–25].

Trace metals in soils and dusts can be accumulated in the human body via direct inhalation, ingestion, and dermal contact absorption or via the soil-crop system. The anthropogenic sources of metals include traffic emission, industrial and domestic emission, atmospheric deposition, mining, waste disposal, sew-

age, pesticides, and fertilizers. Without proper management, abandoned mines will cause more serious environmental impacts compared with active mines [26–28]. Consumption of food crops growing in contaminated area is one of the important sources of human exposure to metals in mining areas [29]. Soil contamination in urban environment by trace metals is of public concerns. For better risk assessment, it is important to determine their background concentrations in urban soils. For instance, Molybdenum (Mo) is an essential trace element for human, animal, and plant health. Mo deficiency in soils has frequently been reported, especially under P-deficient conditions. However, Mo is also a potentially toxic contaminant to soils and aquifers that may pose significant threat to ecological and human health [30].

Another research studied the sources and extent of arsenic (As) contamination and the translocation and speciation from microbes to soil are illustrated [31]. Moreover, several activities can build up soil copper (Cu) concentrations leading to incorporation into the food chain and adversely affect natural and managed ecosystems [32]. The cobalt (Co)-contaminated soil has exposed potential toxicity to humans, plants, and animals. Recently, scientists have summarized the natural and anthropogenic sources arousing the increase of cobalt in soil and review the cobalt species in soil and factors that influence the mobilization of cobalt [33]. Soil contamination in urban environment by trace metals is of public concerns. For better risk assessment, it is important to determine their background concentrations in urban soils. One investigation determined the concentrations of 9 trace metals including As, Ba, Cd, Co, Cu, Ni, Pb, Se, and Zn in 214 urban soils from 6 cities of different sizes from both public and commercial sites in Florida [34].

Remediation using chemical, physical, and biological methods has been adopted to solve the problem. Up to date, phytoremediation approach has affirmed to be a promising viewpoint to traditional methods as it is environmentally friendly, cost effective [17]. Boron nitride nanomaterials have been used owing to their unique characteristics such as eco-friendly attributes for pollutant adsorption, big surface area, high chemical & mechanical strength and semiconducting property [35]. Boron nitride nanometerials usually exhibit semi-leading behavior, which is considered a proper alternative to carbon nanotubes. The properties of boron and nitrogen atoms which are the first neighbors of carbon in the periodic table, make boron nitride as an interesting subject of numerous studies [36]. In recent years, different investigations on the adsorption of chemical contaminants and applying various boron nitride nanomaterials as adsorbents for water purification have been studied [37–39].

Various physical shapes of boron nitride (BN)-based nano adsorbents such as nanoparticles, fullerenes, nanotubes, nanofibers, nanoribbons, nanosheets, nanomeshes, nanoflowers, and hollow spheres have been broadly considered possible adsorbents owing to their exceptional characteristics such as large surface area, structural variability, great chemical/mechanical strength, abundant structural defects, high reactive sites, and functional groups [40]. In this work, B_5N_{10}-nc has been modeled for trapping transition metals of Cr, Mn, Fe, Zn, W, Cd. Physical and chemical properties of the interaction binding between Cr, Mn, Fe, Zn, W, Cd, and boron/ nitrogen in B_5N_{10}-nc have been estimated.

2. THEORY, SUBSTANCES AND APPROACHES

The goal of this research article is to detect and trap the metal, metalloid and nonmetal atoms from soil by using B_5N_{10}-nc. The intention is to remove Cr, Mn, Fe, Zn, W, Cd from the soil medium containing toxic ingredients. The soil medium consists of metal, metalloid and nonmetal atoms and the added B_5N_{10}-nc (Fig. 1). B_5N_{10}-nc was modeled in the presence of Cr, Mn, Fe, Zn, W, Cd through computational methods of density functional method of CAM–B3LYP–D3. The metal, metalloid and nonmetal atoms were successfully incorporated in the center of B_5N_{10}-nc toward formation of Cr $\leftrightarrow$ B_5N_{10}-nc, Mn $\leftrightarrow$ B_5N_{10}-nc, Fe $\leftrightarrow$ B_5N_{10}-nc, Zn $\leftrightarrow$ B_5N_{10}-nc, W $\leftrightarrow$ B_5N_{10}-nc, and Cd $\leftrightarrow$ B_5N_{10}-nc complexes (Fig. 1) and charge distribution of these complexes has been computed owing to the parameter of Bader charge evaluation [41–43]. Irrespective of what element, the B_5N_{10}-nc becomes bigger for embedding these elements.

There are many ions and electrons in a metallic solid which form a many-body system [44–50]. DFT has been performed in this article due to projector/ameliorated/wave method, Perdew/Burke/Ernzerhof functional based on the generalized gradient approximation as the exchange-correlation functional, and non-empirical PBE functional [51–54]. For years, metals and metalloids with computed bandwidths have been an important discussion through DFT [55–58]. In this paper, it has been investigated first principles calculations for trapping transition metals of Cr, Mn, Fe, Zn, W, Cd by B_5N_{10}-nc using DFT methods. The electronic density within the Kohn-Sham (KS) equations leads us to a considerable reduction of quantum computing towards Hamiltonian parameter [59, 60]. Furthermore, B3LYP (Becke, Lee, Yang, Parr) function as a hybrid functional of 3-parameter basis function and LANL2DZ basis set for metals and metalloids within DFT approach [61–67]. In addition, a new hybrid exchange–correlation functional called CAM–B3LYP was suggested which merges B3LYP and the

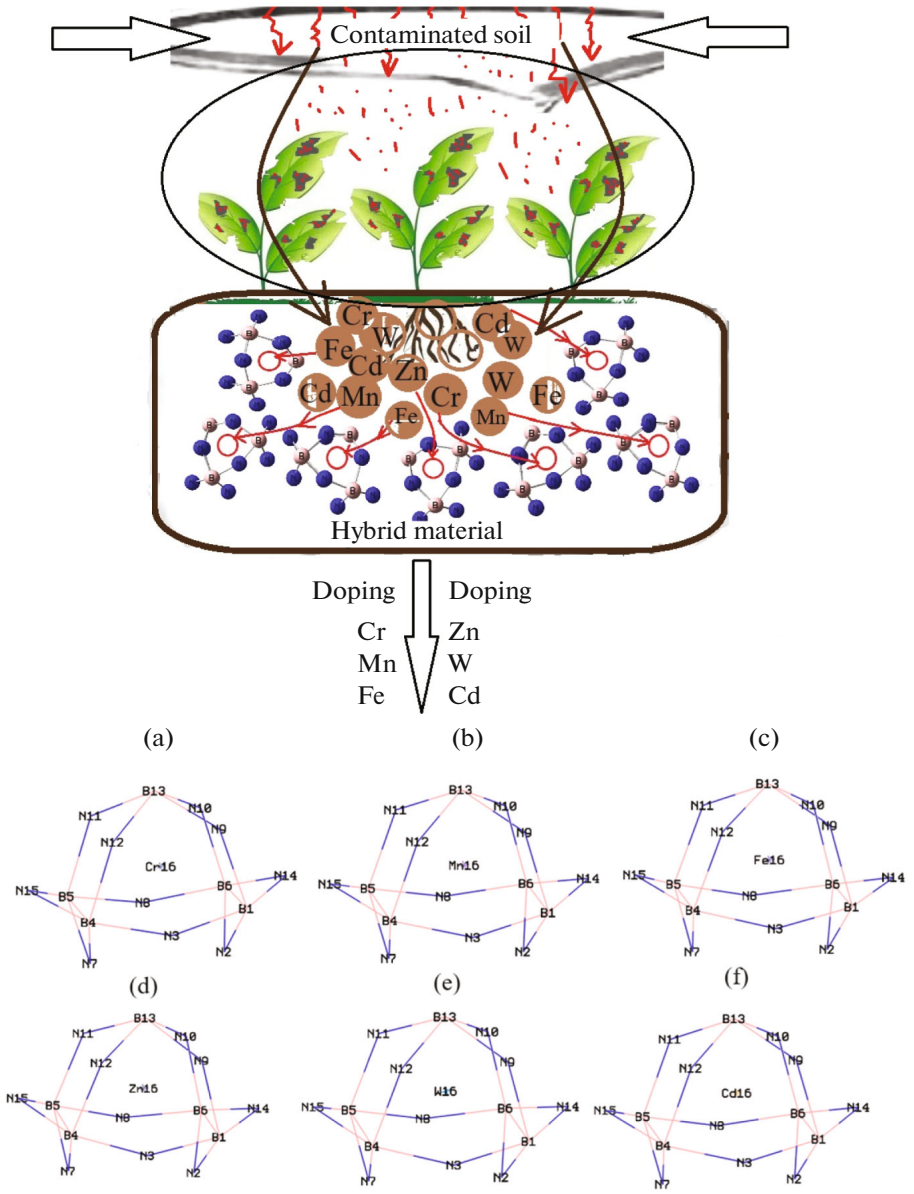

Fig. 1. Trapping of some contaminant elements of Cr, Mn, Fe, Zn, W, Cd in polluted soil via B_5N_{10}-nc and formation of (a) Cr ↔ B_5N_{10}-nc, (b) Mn ↔ B_5N_{10}-nc, (c) Fe ↔ B_5N_{10}-nc, (d) Zn ↔ B_5N_{10}-nc, (e) W ↔ B_5N_{10}-nc, and (f) Cd ↔ B_5N_{10}-nc complexes using CAM–B3LYP–D3/EPR-3, LANL2DZ towards clean soil.

long-range correction. Moreover, the DFT functionals with the Grimme's D3 correction has been considered. The approach of dispersion correction is added to Kohn–Sham density functional theory (DFT-D) with higher accuracy [68–73].

In this work, DFT computations was accomplished by Gaussian 16 revision C.01 program package [74]. The z-matrix coordination has been built for trapping transition metals of Cr, Mn, Fe, Zn, W, Cd in soil by the B_5N_{10}-nc using GaussView 6.1 [75] via the solid model and coordination (Fig. 1). The consequences will remark on the following challenges faced by the DFT approaches in accurately describing the (transition metals) – (boron and nitrogen) bonding [76–86].

3. RESULTS AND DISCUSSION

3.1. Electronic Evaluation & PDOS

The electronic structure of toxic element trapping including Cr, Mn, Fe, Zn, W, Cd using B_5N_{10}-nc has been illustrated using CAM–B3LYP–D3/6–311+G(d, p), LANL2DZ level of theory. Figures 2a–2f) shows the projected density of state (PDOS) of X ↔ B_5N_{10}-nc through Cr, Mn, Fe, Zn, W, Cd encapsulation. The existence of the energy states (*p*-orbital)

of B, N, and (*d*-orbital) of Cr, Mn, Fe, Zn, W, Cd within the gap of X↔B_5N_{10}-nc induces the reactivity of the system. It is clear from the figure that after trapping of transitions metals, there is a significant contribution of *d*-orbital in the unoccupied level. Therefore, the curve of partial PDOS has described that *p* states of B, N atoms in B_5N_{10}-nc and *d*-orbital of X ↔ B_5N_{10}-nc (X = Cr, Mn, Fe, Zn, W, Cd) overcome due to the conduction band (Figs. 2a–2f). A distinguished adsorption trait might be seen in X↔B_5N_{10}-nc because of the potent interaction between the *p* states of boron and nitrogen in B_5N_{10}-nc with *d* states of As, Se, Co, Cu, Mo in X ↔ B_5N_{10}-nc complexes.

Figures 2a–2f shows that Cr ↔ B_5N_{10}-nc, Mn ↔ B_5N_{10}-nc, Fe ↔ B_5N_{10}-nc, Zn ↔ B_5N_{10}-nc, W ↔ B_5N_{10}-nc, and Cd ↔ B_5N_{10}-nc complexes have the most contribution at the middle of the conduction band between −5 to −15 eV, while contribution of boron and nitrogen states are enlarged and similar together, and grabbing of Cr, Mn, Fe, Zn, W, Cd depicts interfacial electronic of the B_5N_{10}-nc for selection of these atoms. Cr ↔ B_5N_{10}-nc has indicated one sharp peak around −10 eV for Cr in Fig. 2a, while Mn ↔ B_5N_{10}-nc (Fig. 2b) has a sharp peak around −5 eV for Mn. The complexes of Fe ↔ B_5N_{10}-nc (Fig. 2c) and Zn ↔ B_5N_{10}-nc (Fig. 2d) have exhibited a sharp peak around −8.5 eV for Fe and Zn atoms, respectively. Furthermore, W ↔ B_5N_{10}-nc (Fig. 2e) has exhibited a strong peak around −10 eV through the graphs for W. Moreover, Cd graph in Cd ↔ B_5N_{10}-nc (Fig. 2f) with a sharp peak around −12.5 eV attracts our attention. As it can be seen, the order potency of atom grabbing of Cr, Mn, Fe, Zn, W, Cd by B_5N_{10}-nc based on the PDOS might be shifted as:

$$\text{Cd} \leftrightarrow B_5N_{10}\text{-nc} > \text{W} \leftrightarrow B_5N_{10}\text{-nc} \approx \text{Cr} \leftrightarrow B_5N_{10}\text{-nc} > \text{Zn} \leftrightarrow B_5N_{10}\text{-nc} \approx \text{Fe} \leftrightarrow B_5N_{10}\text{-nc} \gg \text{Mn} \leftrightarrow B_5N_{10}\text{-nc}.$$

3.2. Theoretical Insight and Analysis of Electric Potential

Nuclear quadrupole is a resonance (NQR) related to nuclear magnetic resonance (NMR) which shows the unsymmetrical distribution of electric charge of a spinning nucleus [87, 88]. All nuclei with a spin number $1 > 1$ have a magnetic moment and an electric quadrupole moment that measures the deviation of the distribution of the positive charge in the nucleus [89, 90]. In this work, the quantum mechanics of NQR at zero-field containing the magnitudes of nuclear quadrupole moments have been carried out on trapping Cr, Mn, Fe, Zn, W, Cd by B_5N_{10}-nc.

Since the electric field gradient (EFG) at the settlement of the nucleus in metal, metalloid and nonmetal atoms including Cr, Mn, Fe, Zn, W, Cd is defined by the valence electrons bent in the pure location with familiar nuclei of B_5N_{10}-nc through trapping of Cr, Mn, Fe, Zn, W, Cd, the frequency of NQR at which intermediates occur is only for X ↔ B_5N_{10}-nc complexes (X = Cr, Mn, Fe, Zn, W, Cd) (Table 1). In the present research, the electric potential via Bader charge was estimated for Cr ↔ B_5N_{10}-nc, Mn ↔ B_5N_{10}-nc, Fe ↔ B_5N_{10}-nc, Zn ↔ B_5N_{10}-nc, W ↔ B_5N_{10}-nc, and Cd ↔ B_5N_{10}-nc complexes (Table 1).

Furthermore, in Figs. 3a–3f), the graph of electric potential fluctuation via Bader charge for toxic transition metals of Cr, Mn, Fe, Zn, W, Cd grabbed by the B_5N_{10}-nc (Fig. 1) have been assessed. In Figs. 3a–3f, the trapping fluctuation of Cr, Mn, Fe, Zn, W, Cd by B_5N_{10}-nc for sensing the toxic metal, metalloid and nonmetal atoms in the contaminated soil can be observed. The graph of B_5N_{10}-nc is bent by these toxic atoms. The sharpest curves for electric potential were nominated for metal, metalloid and nonmetal atoms trapped by the B_5N_{10}-nc that prove the electron attaining of these elements aided by boron and nitrogen atoms of B_5N_{10}-nc based on the relation coefficient of R^2 as:

$$\text{Cd} \leftrightarrow B_5N_{10}\text{-nc} > \text{Zn} \leftrightarrow B_5N_{10}\text{-nc} \approx \text{Cr} \leftrightarrow B_5N_{10}\text{-nc} > \text{Fe} \leftrightarrow B_5N_{10}\text{-nc} > \text{Mn} \leftrightarrow B_5N_{10}\text{-nc} > \text{W} \leftrightarrow B_5N_{10}\text{-nc},$$

(see Figs. 3a–3f).

3.3. Background and Application of Nuclear Magnetic Resonance

The investigation of application of nuclear magnetic resonance (NMR) of high- materials and other correlated-electron systems improved for conventional superconductors and d-band transition metals, alloys, and intermetallic compounds [91, 92]. As a matter of fact, magnetic field gradients fix it feasible to tag spatial coordinates within a model. The frequencies resonance of most atoms is well segregated from each other which causes NMR to be an element-specific method. Interactions of spins with their local environment direct spectral alterations that evoke the local geometry and physico-chemical states. Therefore, NMR spectrum of B_5N_{10}-nc for trapping metal, metalloid and nonmetal atoms containing Cr, Mn, Fe, Zn, W, Cd might illustrate the possibility of B_5N_{10}-nc for sensing and grabbing of these toxic elements from contaminated soil toward measuring the isotropic chemical-shielding (CSI) and anisotropic chemical-shielding (CSA). The NMR quantities of isotropic (σ_{iso}) and anisotropic shielding tensor (σ_{aniso}) of Ba, As, Se, Co, Cu, Mo trapped on the in the B_5N_{10}-nc towards formation of Cr ↔ B_5N_{10}-nc, Mn ↔ B_5N_{10}-nc, Fe ↔ B_5N_{10}-nc, Zn ↔ B_5N_{10}-nc, W ↔ B_5N_{10}-nc, and Cd ↔ B_5N_{10}-nc complexes was computed by Gaussian 16 revision C.01 program package (Table 2) [74].

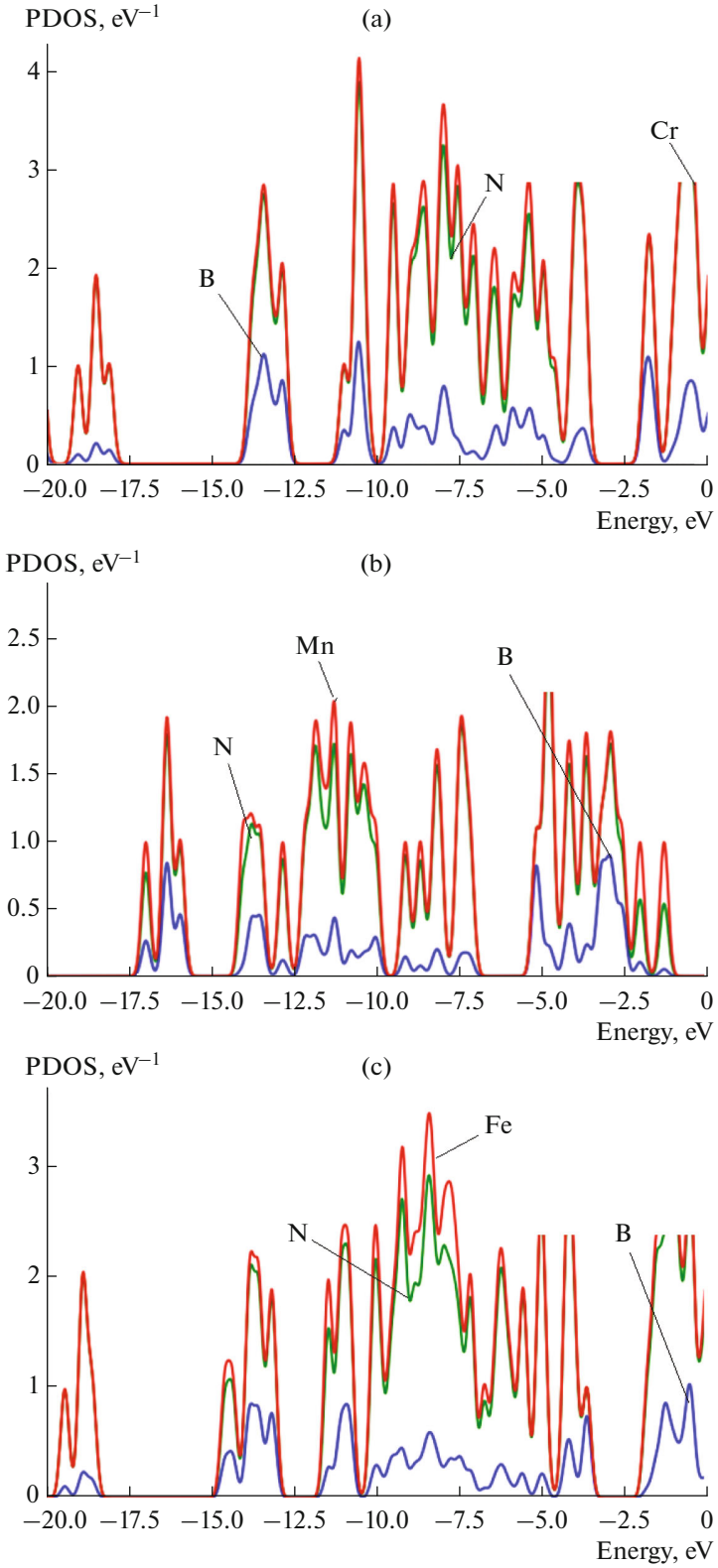

Fig. 2. PDOS encapsulation of transition metals by B_5N_{10}-nc toward formation of complexes including (a) Cr ↔ B_5N_{10}-nc, (b) Mn ↔ B_5N_{10}-nc, c) Fe ↔ B_5N_{10}-nc, (d) Zn ↔ B_5N_{10}-nc, (e) W ↔ B_5N_{10}-nc, and (f) Cd ↔ B_5N_{10}-nc by CAM–B3LYP–D3/6–311+G(d, p), LANL2DZ.

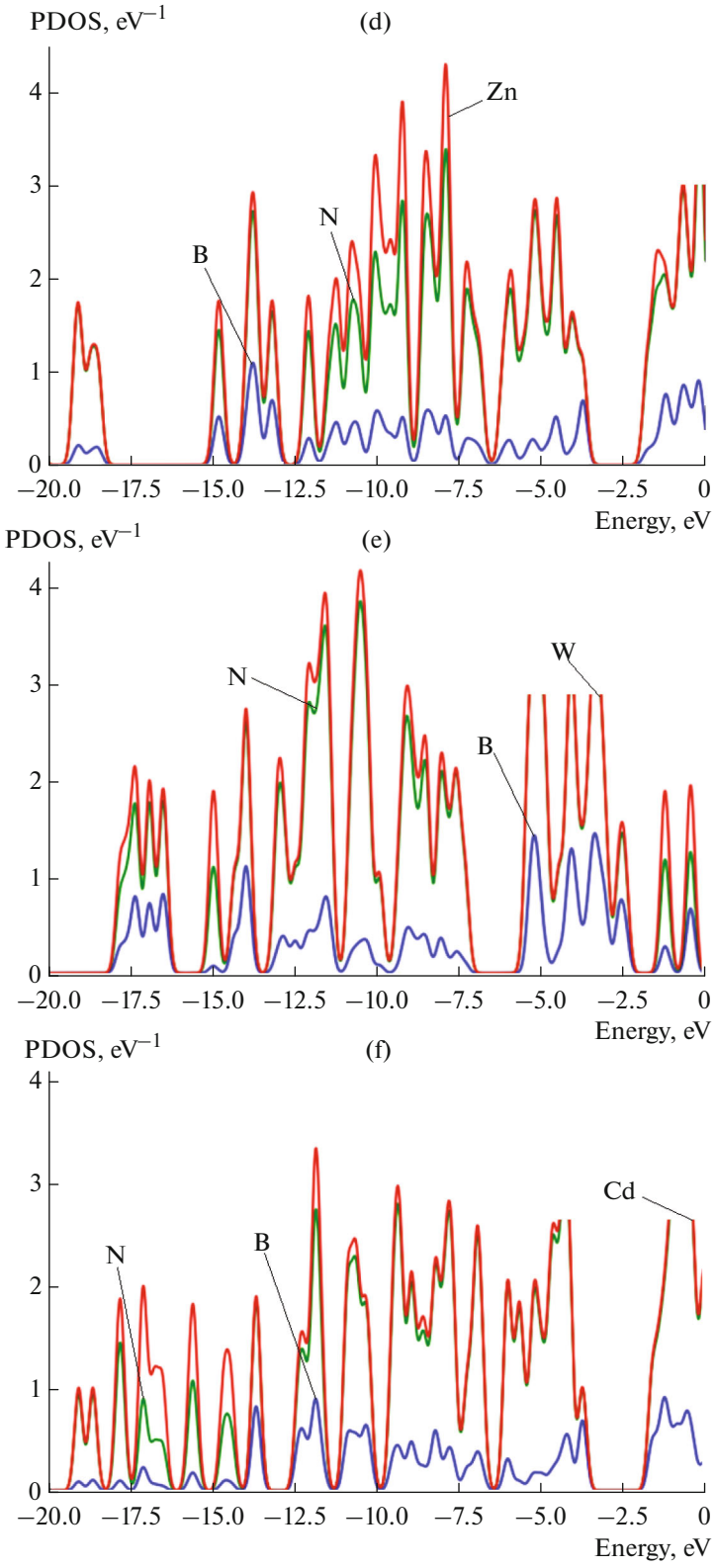
PDOS, eV^{-1}
(d)
Zn
N
B
Energy, eV
PDOS, eV^{-1}
(e)
N
W
B
Energy, eV
PDOS, eV^{-1}
(f)
Cd
N
B
Energy, eV

Fig. 2. (Contd.)

Table 1. The amounts of electric potential (E_p /a.u.) and Bader charge (Q /coulomb) through NQR calculation for Cr ↔ B_5N_{10}-nc, Mn ↔ B_5N_{10}-nc, Fe ↔ B_5N_{10}-nc, Zn ↔ B_5N_{10}-nc, W ↔ B_5N_{10}-nc, and Cd ↔ B_5N_{10}-nc complexes

Cr ↔ B_5N_{10}-nc			Mn ↔ B_5N_{10}-nc			Fe ↔ B_5N_{10}-nc		
atom	Q	E_p	atom	Q	E_p	atom	Q	E_p
B1	0.28	−11.24	B1	0.19	−11.22	B1	0.27	−11.24
N2	−0.20	−18.10	N2	−0.05	−18.28	N2	−0.18	−18.10
N3	−0.25	−18.11	N3	−0.16	−18.30	N3	−0.25	−18.11
B4	0.33	−11.23	B4	0.20	−11.21	B4	0.31	−11.24
B5	0.32	−11.24	B5	0.22	−11.21	B5	0.31	−11.24
B6	0.32	−11.22	B6	0.20	−11.21	B6	0.28	−11.24
N7	−0.20	−18.11	N7	−0.05	−18.28	N7	−0.17	−18.10
N8	−0.27	−18.12	N8	−0.16	−18.29	N8	−0.24	−18.11
N9	−0.34	−18.14	N9	−0.05	−18.29	N9	−0.36	−18.14
N10	−0.31	−18.13	N10	−0.05	−18.29	N10	−0.32	−18.14
N11	−0.29	−18.14	N11	−0.07	−18.30	N11	−0.27	−18.13
N12	−0.36	−18.13	N12	−0.10	−18.29	N12	−0.40	−18.13
B13	0.11	−11.24	B13	0.30	−11.22	B13	−0.02	−11.27
N14	−0.16	−18.09	N14	−0.11	−18.29	N14	−0.13	−18.08
N15	−0.17	−18.11	N15	−0.14	−18.29	N15	−0.16	−18.09
Cr16	1.20	−101.75	Mn16	−0.17	−16.56	Fe16	1.35	−113.90
Zn ↔ B_5N_{10}-nc			W ↔ B_5N_{10}-nc			Cd ↔ B_5N_{10}-nc		
atom	Q	E_p	atom	Q	E_p	atom	Q	E_p
B1	0.28	−11.25	B1	0.20	−11.22	B1	0.27	−11.24
N2	−0.23	−18.12	N2	−0.07	−18.29	N2	−0.24	−18.13
N3	−0.21	−18.10	N3	−0.21	−18.31	N3	−0.22	−18.09
B4	0.32	−11.24	B4	0.23	−11.21	B4	0.32	−11.24
B5	0.31	−11.24	B5	0.25	−11.21	B5	0.30	−11.25
B6	0.30	−11.24	B6	0.23	−11.21	B6	0.29	−11.24
N7	−0.19	−18.11	N7	−0.04	−18.29	N7	−0.22	−18.13
N8	−0.22	−18.10	N8	−0.20	−18.30	N8	−0.23	−18.10
N9	−0.31	−18.13	N9	−0.20	−18.31	N9	−0.33	−18.13
N10	−0.29	−18.14	N10	−0.19	−18.31	N10	−0.32	−18.14
N11	−0.26	−18.13	N11	−0.21	−18.30	N11	−0.27	−18.14
N12	−0.37	−18.13	N12	−0.22	−18.31	N12	−0.40	−18.13
B13	0.06	−11.24	B13	0.43	−11.23	B13	0.05	−11.20
N14	−0.17	−18.11	N14	−0.03	−18.28	N14	−0.17	−18.11
N15	-0.16	−18.10	N15	−0.07	−18.28	N15	−0.15	−18.10
Zn16	1.16	−139.88	W16	0.11	−10.33	Cd16	1.33	−268.15

Table 2 has reported NMR amounts for transition metals of Cr, Mn, Fe, Zn, W, Cd encapsulated in the B_5N_{10}-nc. Grabbing Cr, Mn, Fe, Zn, W, Cd shows the spin polarization on the (Cr, Mn, Fe, Zn, W, Cd)–encapsulated B_5N_{10}-nc. The increase in the chemical shift anisotropy spans for atom trapping by the B_5N_{10}-nc are near N(2, N3, N7, N8, N9, N10, N11, N12, N14 and N15 (Table 2). The observed weak signal intensity near the parallel edge of the nanocage might be owing to boron binding induced non-spherical distribution of these complexes. It is obvious that grabbing Cr, Mn, Fe, Zn, W, Cd by B_5N_{10}-nc might promote the strength of the nanocage that concludes an increase in the magnetic of clusters (Table 2).

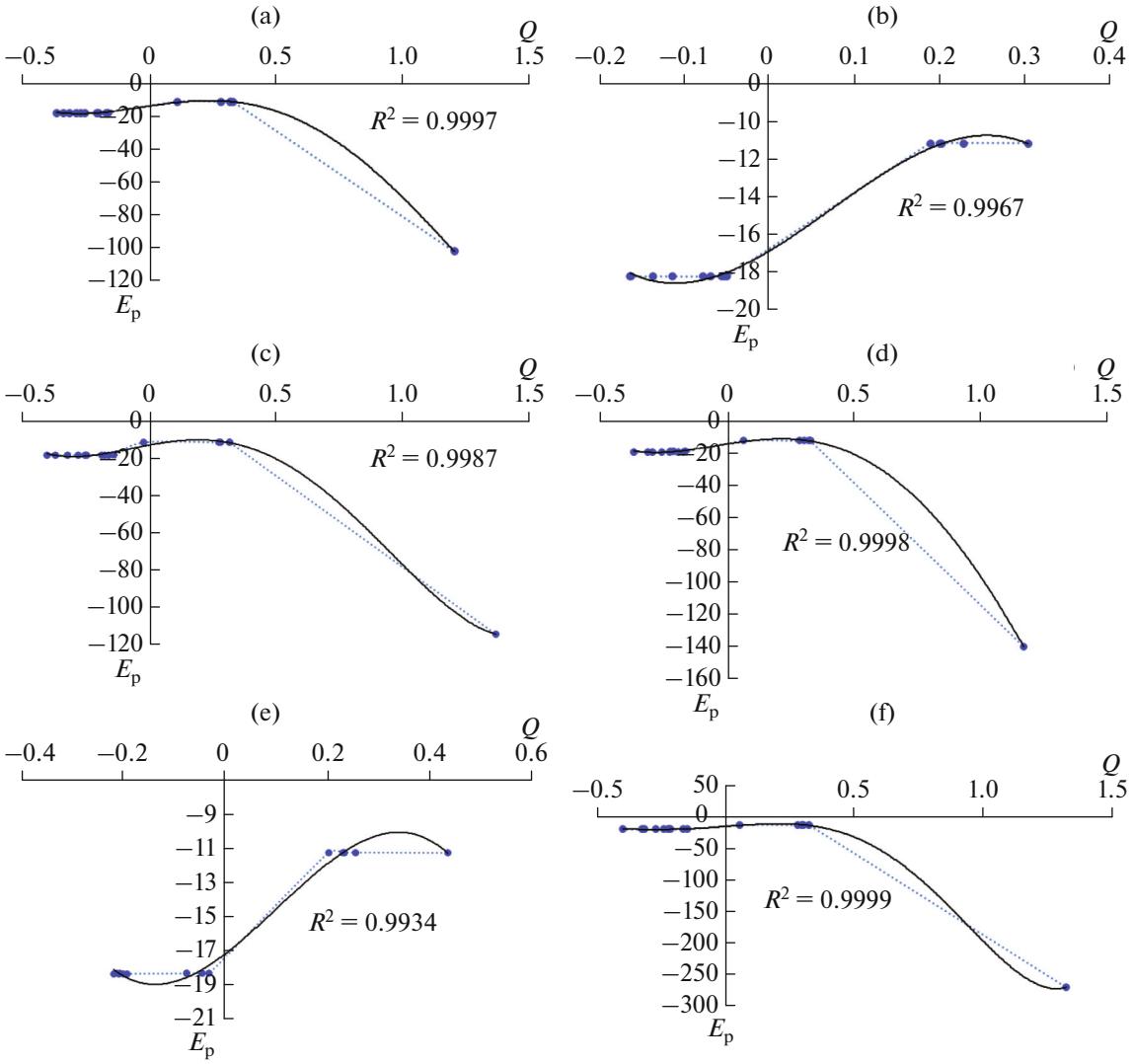

Fig. 3. The amounts of electric potential (E_p/a.u.) versus Bader charge (Q/coulomb) through NQR calculation for complexes of (a) Cr ↔ B_5N_{10}-nc, b) Mn ↔ B_5N_{10}-nc, (c) Fe ↔ B_5N_{10}-nc, (d) Zn ↔ B_5N_{10}-nc, (e) W ↔ B_5N_{10}-nc, and (f) Cd ↔ B_5N_{10}-nc.

Figures 4a–4f indicated the same desire of shielding factor for boron and nitrogen; however, a remarkable deviation is observed from trapping atoms of Cr16 (Fig. 4a), Mn16 (Fig. 4b), Fe16 (Fig. 4c), Zn16 (Fig. 4d), W16 (Fig. 4e), Cd16 (Fig. 4f) through interaction with boron and nitrogen of B_5N_{10}-nc. In Figs. 4a–4f, toxic elements of Cr, Mn, Fe, Zn, W, Cd in the complexes of Cr ↔ B_5N_{10}-nc (Fig. 4a), Mn ↔ B_5N_{10}-nc (Fig. 4b), Fe ↔ B_5N_{10}-nc (Fig. 4c), Zn ↔ B_5N_{10}-nc (Fig. 4d), W ↔ B_5N_{10}-nc (Fig. 4e), and Cd ↔ B_5N_{10}-nc (Fig. 4f) describe the oscillation in the chemical shielding during atom capture.

Figures 4a–4f defines the chemical shielding between boron/nitrogen in B_5N_{10}-nc and metal, metalloid and nonmetal atoms. Thus, it may be brought up that the turnover of electron admitting for the captured toxic atoms in the B_5N_{10}-nc is

$$Cd > Zn > Fe > Mn > Cr \approx W,$$

that proves the strength of covalent bond across boron/nitrogen and these elements toward atom catching. The curves of metal, metalloid and nonmetal elements of Cr, Mn, Fe, Zn, W, Cd through the trapping in the B_5N_{10}-nc during atom detection and removal from soil.

3.4. Interpreting Infrared Spectra

Trapping metal, metalloid and nonmetal elements of Cr, Mn, Fe, Zn, W, Cd in the B_5N_{10}-nc has been evaluated by interpreting infrared (IR) spectroscopy [93] during atom sensing in soil. The complexes of Cr ↔ B_5N_{10}-nc (Fig. 5a), Mn ↔ B_5N_{10}-nc (Fig. 5b), Fe ↔ B_5N_{10}-nc (Fig. 5c), Zn ↔ B_5N_{10}-nc (Fig. 5d), W ↔ B_5N_{10}-nc (Fig. 5e), and Cd ↔ B_5N_{10}-nc (Fig. 5f)

Table 2. Data of NMR shielding tensors for selected atoms of Cr ↔ B_5N_{10}-nc, Mn ↔ B_5N_{10}-nc, Fe ↔ B_5N_{10}-nc, Zn ↔ B_5N_{10}-nc, W ↔ B_5N_{10}-nc, and Cd ↔ B_5N_{10}-nc complexes using CAM–B3LYP–D3/LANL2DZ calculations

Cr ↔ B_5N_{10}-nc			Mn ↔ B_5N_{10}-nc			Fe ↔ B_5N_{10}-nc		
atom	σ_{iso}	σ_{aniso}	atom	σ_{iso}	σ_{aniso}	atom	σ_{iso}	σ_{aniso}
B1	117.00	83.08	B1	93.19	74.33	B1	136.16	112.12
N2	99.88	287.95	N2	107.17	412.45	N2	252.73	554.33
N3	38.33	429.47	N3	288.84	780.64	N3	163.84	480.57
B4	109.56	90.41	B4	98.46	54.76	B4	137.86	110.52
B5	104.41	97.35	B5	80.47	75.44	B5	125.17	101.47
B6	84.15	70.38	B6	80.82	69.26	B6	137.05	99.38
N7	65.83	250.69	N7	111.05	258.37	N7	76.06	523.93
N8	173.42	711.36	N8	359.39	935.99	N8	5.14	118.99
N9	228.26	477.97	N9	390.09	580.18	N9	11.83	408.43
N10	297.35	970.54	N10	353.08	404.20	N10	15.62	277.72
N11	112.15	469.82	N11	122.89	484.16	N11	8.18	651.24
N12	146.15	520.75	N12	126.01	403.80	N12	40.82	366.00
B13	23.41	161.67	B13	51.76	125.50	B13	92.95	56.18
N14	61.43	542.28	N14	390.19	1289.60	N14	137.87	620.38
N15	144.21	582.40	N15	281.07	1330.18	N15	66.25	524.60
Cr16	8.81	531.86	Mn16	4675.24	3740.24	Fe16	982.38	1080.91
Zn ↔ B_5N_{10}-nc			W ↔ B_5N_{10}-nc			Cd ↔ B_5N_{10}-nc		
atom	σ_{iso}	σ_{aniso}	atom	σ_{iso}	σ_{aniso}	atom	σ_{iso}	σ_{aniso}
B1	130.51	91.88	B1	91.70	68.85	B1	127.30	98.78
N2	21.68	546.01	N2	23.40	244.56	N2	14.31	556.00
N3	56.01	57.53	N3	223.66	505.27	N3	13.41	122.46
B4	120.38	53.04	B4	92.23	72.95	B4	103.12	115.33
B5	115.01	68.56	B5	81.61	72.35	B5	118.25	61.95
B6	133.63	81.25	B6	79.37	80.41	B6	123.67	80.88
N7	1.32	478.38	N7	67.14	230.36	N7	131.61	549.60
N8	51.13	184.30	N8	331.07	856.46	N8	19.87	130.06
N9	134.42	330.98	N9	454.05	614.22	N9	97.35	203.87
N10	55.07	270.09	N10	432.20	652.74	N10	41.26	585.38
N11	35.54	334.95	N11	276.32	480.30	N11	26.81	253.29
N12	166.18	238.32	N12	133.37	462.91	N12	25.73	620.63
B13	126.72	17.46	B13	17.50	225.23	B13	139.30	55.84
N14	32.39	478.12	N14	413.15	983.42	N14	47.77	423.76
N15	104.95	596.10	N15	381.90	1002.60	N15	92.93	392.12
Zn16	2920.24	3680.66	W16	37.92	77.29	Cd16	3945.35	242.54

have been analyzed through the IR spectroscopy. The graph of Fig. 5a has been shown in the frequency about 200–1800 cm^{-1} for Cr ↔ B_5N_{10}-nc with several sharp peaks around 655.26, 691.58, and 714.46 cm^{-1}. Then, Fig. 5b was shown in the frequency limitation across 200–1100 cm^{-1} for Mn ↔ B_5N_{10}-nc with several sharp peaks around 567.21, 616.88, 623.54, and 680.89 cm^{-1}. Figure 5c has indicated the frequency around 1800–1100 cm^{-1} for Fe ↔ B_5N_{10}-nc with one sharp peak around 983.42 cm^{-1}. Figure 5d has shown the fluctuation frequency between 50–950 cm^{-1} for Zn ↔ B_5N_{10}-nc with two sharp peaks around 537.66 and 902.68 cm^{-1}. Figure 5e has indicated the fluctuation of frequency between 200–1400 cm^{-1} for W ↔ B_5N_{10}-nc with several

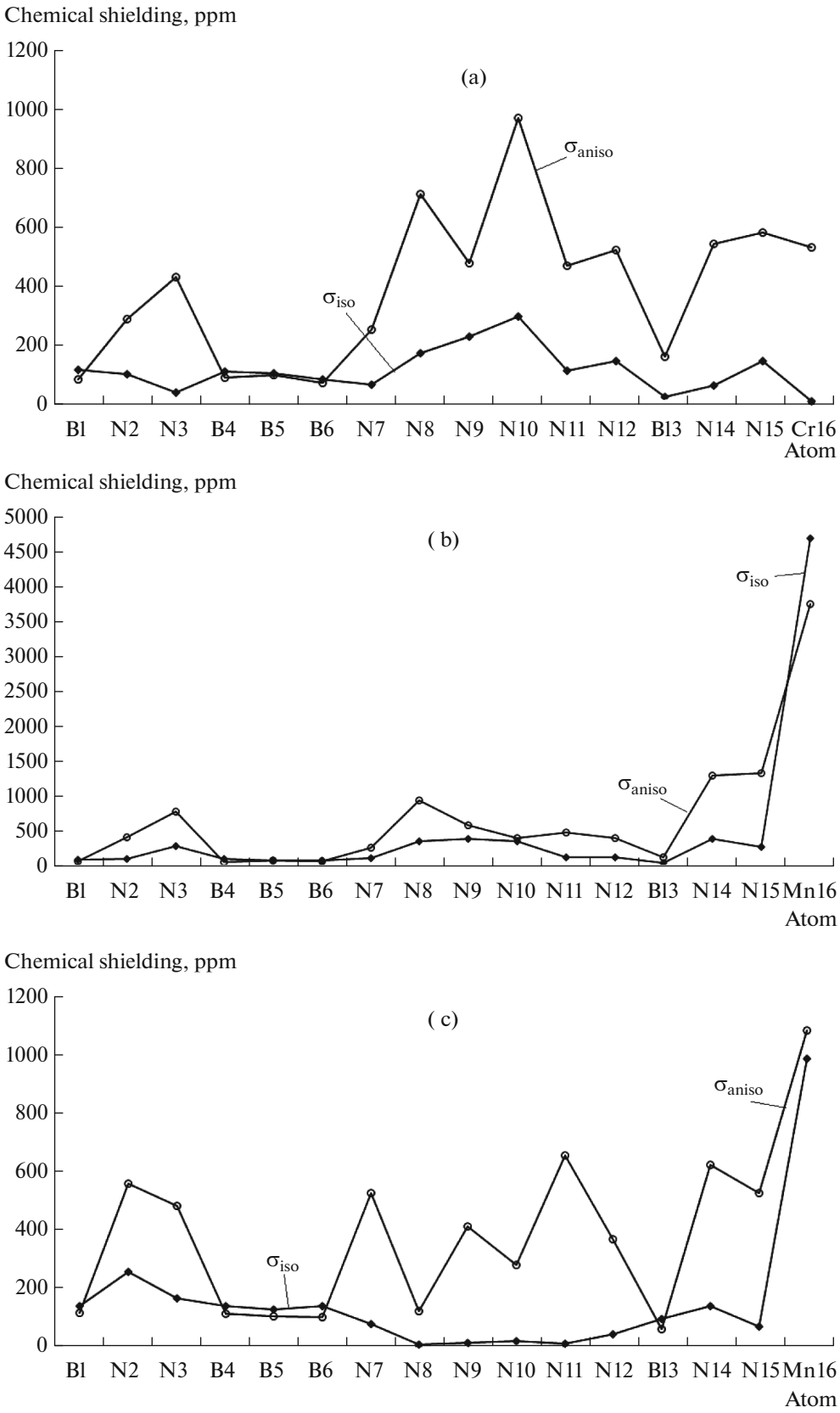

Fig. 4. The NMR spectrum for complexes of (a) Cr ↔ B_5N_{10}-nc, (b) Mn ↔ B_5N_{10}-nc, c) Fe ↔ B_5N_{10}-nc, (d) Zn ↔ B_5N_{10}-nc, (e) W ↔ B_5N_{10}-nc, and (f) Cd ↔ B_5N_{10}-nc using CAM–B3LYP–D3/LANL2DZ.

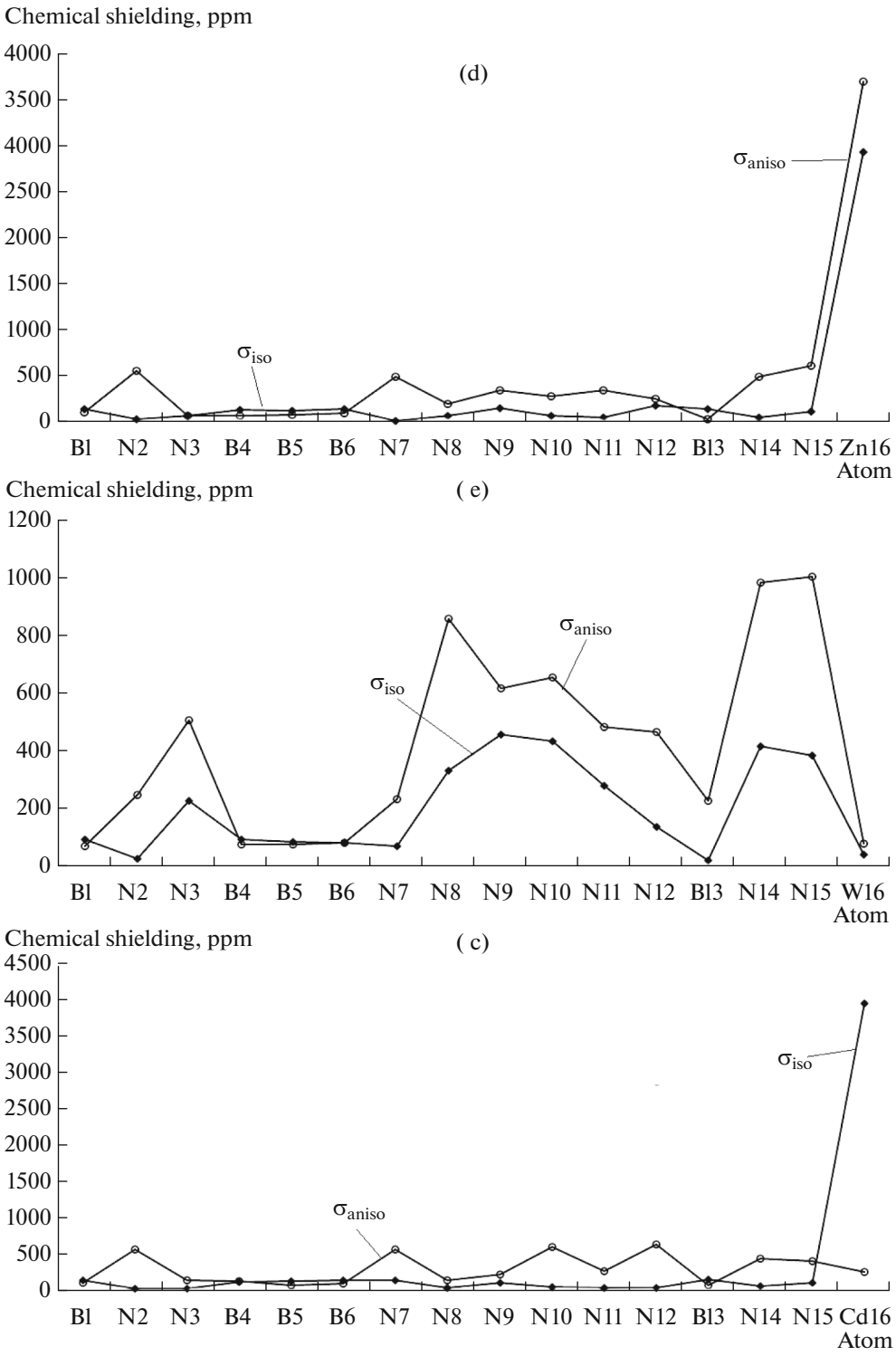

Fig. 4. (Contd.)

sharp peaks around 582.28, 656.11, 664.63, 723.76, and 798.39 cm^{-1}. Figure 5f has shown the frequency range between 100–1600 cm^{-1} for Cd ↔ B_5N_{10}-nc with several sharp peaks around 504.75, 1002.32, and 1233.14 cm^{-1}. Table 3 has described that B_5N_{10}-nc owing to capture transition metals including Cr, Mn, Fe, Zn, W, Cd might be more efficient detector for sensing and catching these elements from soil.

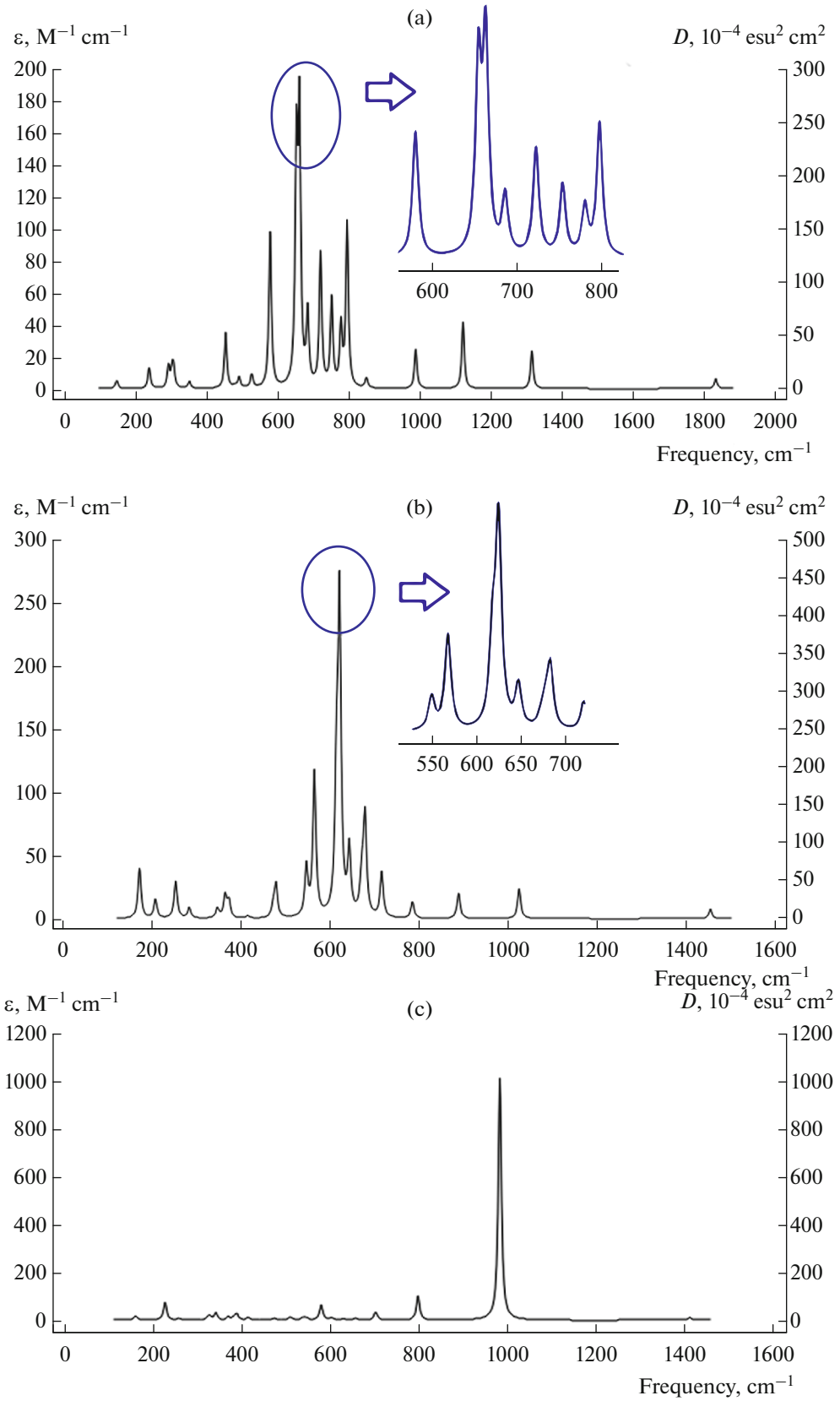

Fig. 5. IR spectra for complexes of (a) Cr ↔ B_5N_{10}-nc, (b) Mn ↔ B_5N_{10}-nc, (c) Fe ↔ B_5N_{10}-nc, (d) Zn ↔ B_5N_{10}-nc, (e) W ↔ B_5N_{10}-nc, and (f) Cd ↔ B_5N_{10}-nc complexes. [Note: ε (M^{-1} cm^{-1}) is the absorbance unit and D (10^{-4} esu^2 cm^2) is the dipole strength via the esu or electrostatic unit, which is a unit of charge in the cgs (centimeter-gram-second system).

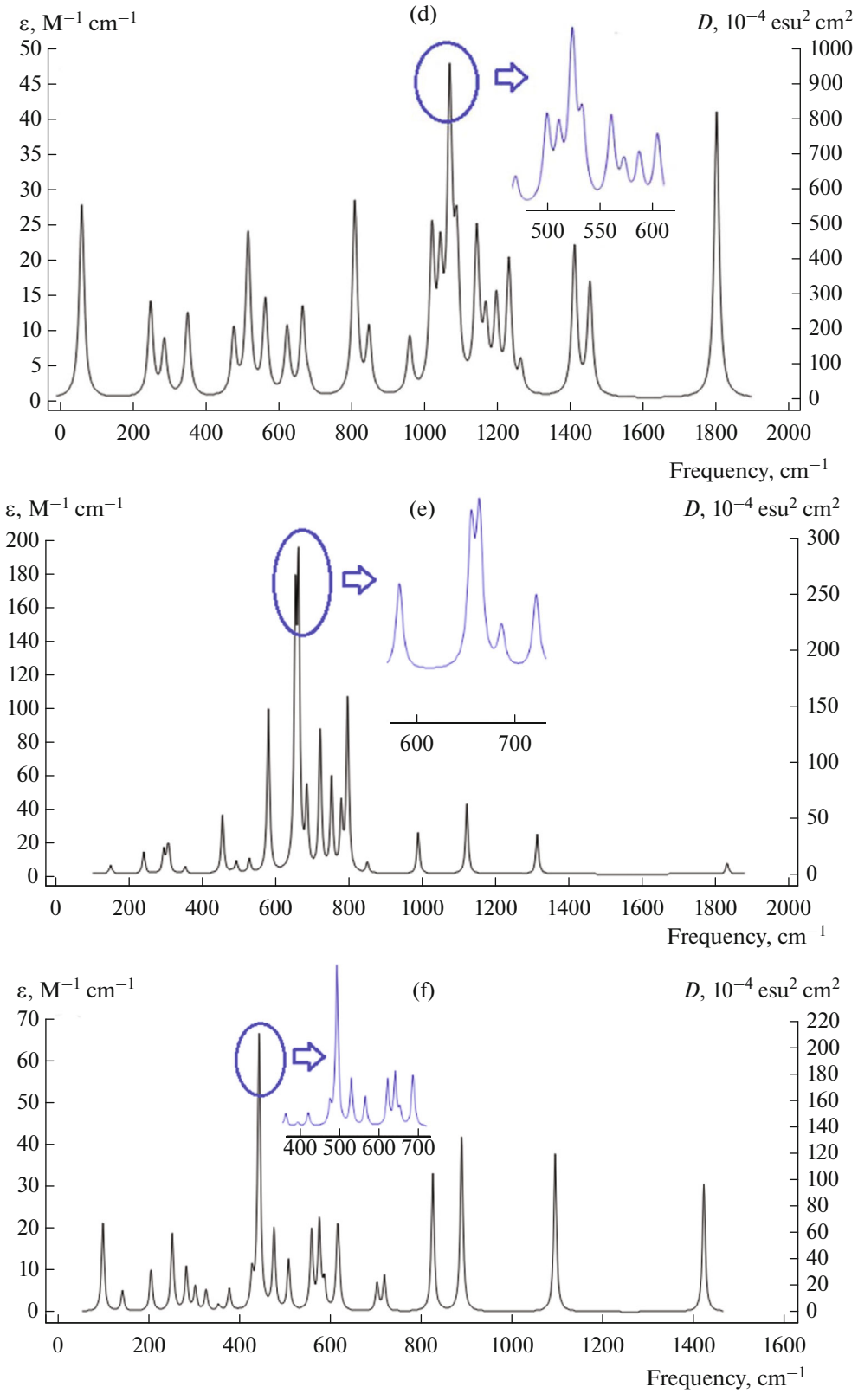
(d)
ε, M^{-1} cm^{-1}
D, 10^{-4} esu^2 cm^2
Frequency, cm^{-1}
(e)
ε, M^{-1} cm^{-1}
D, 10^{-4} esu^2 cm^2
Frequency, cm^{-1}
(f)
ε, M^{-1} cm^{-1}
D, 10^{-4} esu^2 cm^2
Frequency, cm^{-1}

Fig. 5. (Contd.)

Table 3. The thermochemical characters of Cr ↔ B_5N_{10}-nc, Mn ↔ B_5N_{10}-nc, Fe ↔ B_5N_{10}-nc, Zn ↔ B_5N_{10}-nc, W ↔ B_5N_{10}-nc, and Cd ↔ B_5N_{10}-nc complexes

Compound	Dipole moment, D	$\Delta E^o \times 10^{-3}$, kcal/mol	$\Delta H^o \times 10^{-3}$, kcal/mol	$\Delta G^o \times 10^{-3}$, kcal/mol	S^o, cal/K mol
B_5N_{10}-nc	0.2020	−420.550	−420.549	−420.579	100.650
Cr ↔ B_5N_{10}-nc	0.6941	−1063.754	−1063.754	−1063.782	94.375
Mn ↔ B_5N_{10}-nc	0.4888	−485.602	−485.602	−485.629	90.852
Fe ↔ B_5N_{10}-nc	1.4484	−1199.586	−1199.585	−1199.614	95.351
Zn ↔ B_5N_{10}-nc	0.9416	−1518.749	−1518.748	−1518.780	105.321
W ↔ B_5N_{10}-nc	0.5946	−462.747	−462.746	−462.774	90.867
Cd ↔ B_5N_{10}-nc	0.7560	−3811.957	−3811.957	−3811.985	93.836

Table 3 could introduce the ability of metal, metalloid and nonmetal elements of Cr, Mn, Fe, Zn, W, Cd trapped in the B_5N_{10}-nc through ΔG^o_{ads} which is related to the covalent bond between these elements and B_5N_{10}-nc as a potent detector for soil purification. The trapping process of metal, metalloid and nonmetal elements including Cr, Mn, Fe, Zn, W, Cd in the B_5N_{10}-nc is affirmed by the ΔG^o_{ads} quantities:

$$\Delta G^o_{ads} = \Delta G^o_{X\leftrightarrow B5N10-nc} - \left(\Delta G^o_{X-grabbed} + \Delta G^o_{B_5N_{10}-nc}\right);$$
$$X = Cr, Mn, Fe, Zn, W, Cd.$$

Furthermore, Fig. 6 has shown that the dependence on the size of the atoms of during interaction between the adsorbates of the metal, metalloid and nonmetal elements as the electron acceptors and the adsorbent of B_5N_{10}-nc as electron donor in the complexes of Cr ↔ B_5N_{10}-nc, Mn ↔ B_5N_{10}-nc, Fe ↔ B_5N_{10}-nc, Zn ↔ B_5N_{10}-nc, W↔B_5N_{10}-nc, and Cd ↔ B_5N_{10}-nc. Therefore, the selectivity of the metal, metalloid and nonmetal elements by B_5N_{10}-nc (atom sensor) can be resulted as:

$$Cd > Zn > Fe > Cr > Mn \approx W,$$

(see Table 3 and Fig. 6).

CONCLUSIONS

B_5N_{10}-nc can be used to capture metal, metalloid and nonmetal elements from soil because of electrostatic interactions between metal, metalloid and nonmetal elements and B_5N_{10}-nc. The thermochemistry and electromagnetic parameters of Cr, Mn, Fe, Zn,

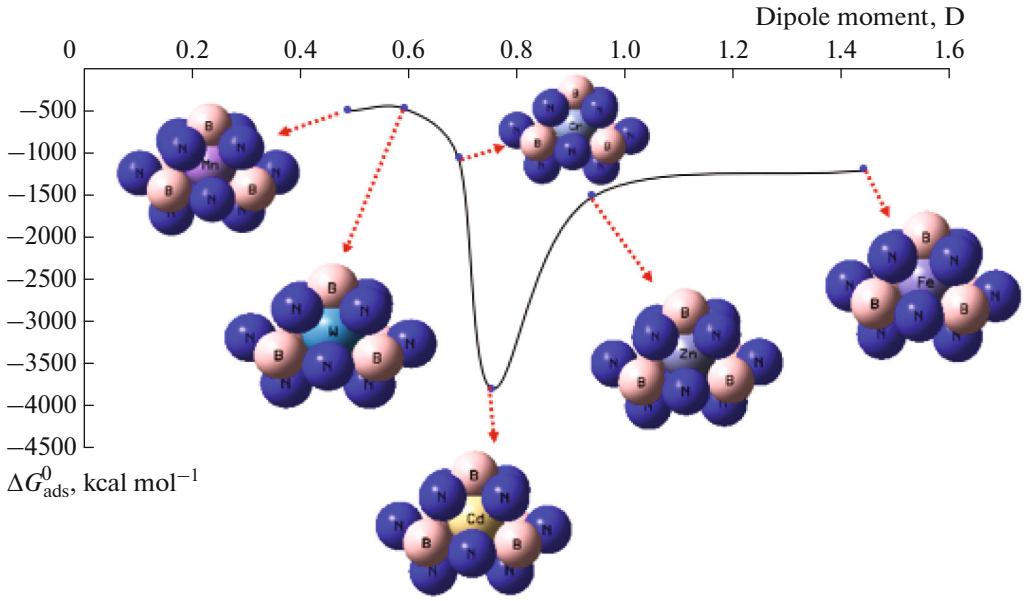

Fig. 6. Gibbs free energy (ΔG^o_{ads}) for Cr ↔ B_5N_{10}-nc, Mn ↔ B_5N_{10}-nc, Fe ↔ B_5N_{10}-nc, Zn ↔ B_5N_{10}-nc, W ↔ B_5N_{10}-nc, and Cd ↔ B_5N_{10}-nc complexes using CAM–B3LYP–D3/6-311+G(d, p), LANL2DZ.

W, Cd absorbed B_5N_{10}-nc has been illustrated by DFT method. The consequences have defined that Cr, Mn, Fe, Zn, W, Cd trapped in B_5N_{10}-nc are rather fixed with the most stable adsorption site being in the center of B_5N_{10}-nc system. Catching Cr, Mn, Fe, Zn, W, Cd in the B_5N_{10}-nc happens due to chemisorption phenomenon. The n-grabbing behavior can be found in B_5N_{10}-nc after the adsorption of Cr, Mn, Fe, Zn, W, Cd. The work function of B_5N_{10}-nc has remarkably exhibited the transition metals adsorption with maximum amount for the Cd > Zn > Fe > Cr > Mn ≈ W – adsorbed B_5N_{10}-nc system. Moreover, it is proposed that transition metals-adsorbed can be employed to design and progress the optoelectronic specification of B_5N_{10}-nc for inventing photoelectric instruments.

ACKNOWLEDGMENTS

In successfully completing this paper and its research, the authors are grateful to Kastamonu University.

FUNDING

This work was supported by ongoing institutional funding. No additional grants to carry out or direct this particular research were obtained.

CONFLICT OF INTEREST

The authors of this work declare that they have no conflicts of interest.

REFERENCES

1. M. Monajjemi, F. Mollaamin, S. Shahriari, et al., Russ. J. Phys. Chem. B **18**, 1090–1112 (2024). https://doi.org/10.1134/S1990793124700465
2. F. Mollaamin and M. Monajjemi, Russ. J. Phys. Chem. B **18**, 533–548 (2024). https://doi.org/10.1134/S199079312402012X
3. Sh. B. Utamuradova, Sh. Kh. Daliyev, K. M. Fayzullayev, et al., New Mater. Compd. Appl. **7**, 37–43 (2023)
4. F. Mollaamin and M. Monajjemi, Comput. Theor. Chem. **1237**, 114666 (2024). https://doi.org/10.1016/j.comptc.2024.114666
5. K. V. Zolotarev, A. N. Mikhailov, V. I. Nakhod, et al., New Mater. Compd. Appl. **8**, 162–170 (2024). https://doi.org/10.62476/nmca82162
6. F. Mollaamin and M. Monajjemi, J. Mol. Struct. **1300**, 137214 (2024). https://doi.org/10.1016/j.molstruc.2023.137214
7. F. B. Eshqurbonov and E. R. Safarova, New Mater. Compd. Appl. **7** (2), 137–148(2023)
8. F. Mollaamin and M. Monajjemi, Sens. Rev. **44**, 179–193 (2024). https://doi.org/10.1108/SR-01-2024-0066
9. S. H. Jabarov, A. Kh. Nabiyeva, S. V. Trukhanov, et al., New Mater. Compd. Appl. **7** (3), 149-155(2023)
10. F. Mollaamin and M. Monajjemi, Russ. J. Phys. Chem. B **18**, 49–66 (2024). https://doi.org/10.1134/S1990793124010159
11. B. Abdullayev, J. Makhmayorov, Z. Ro'ziyeva, et al., New Mater. Compd. Appl. **7** (3), 188–193 (2023).
12. F. Mollaamin and M. Monajjemi, Int. J. Quantum Chem. **124**, e27348 (2024). https://doi.org/10.1002/qua.27348
13. M. F. Thanoon and L. M. Al-Nema, New Mater. Compd. Appl. **8**, 233–243 (2024). https://doi.org/10.62476/nmca82233
14. Mollaamin and M. Monajjemi, Mol. Simulat. **49**, 365 (2023). https://doi.org/10.1080/08927022.2022.2159996
15. R. A. Dawoud, R. S. Shehata, H. Moawod, et al., New Mater. Compd. Appl. **8**, 43–61 (2024). https://doi.org/10.62476/nmca8143
16. W. A. Salih and A. Al-Taie, New Mater. Compd. Appl. **8**, 199–122 (2024). https://doi.org/10.62476/nmca82199
17. C. Li, K. Zhou, W. Qin, et al., Soil Sediment Contam.: Int. J. **28**, 380–394 (2019). https://doi.org/10.1080/15320383.2019.1592108
18. M. N. Boumezrag, K. Almi, S. Lakel, et al., Russ. J. Phys. Chem. B **18**, 873–894 (2024). https://doi.org/10.1134/S1990793124700313
19. M. L. Busurina, A. E. Sytschev, S. G. Vadchenko, et al., Russ. J. Phys. Chem. B **18**, 1002–1008 (2024). https://doi.org/10.1134/S1990793124700544
20. M. N. Boumezrag, K. Almi, S. Lakel, et al., Russ. J. Phys. Chem. B **18**, 895–906 (2024). https://doi.org/10.1134/S1990793124700325
21. I. V. Kumpanenko, N. A. Ivanova, O. V. Shapovalova, et al., Russ. J. Phys. Chem. B **16**, 917–925 (2022). https://doi.org/10.1134/S1990793122050050
22. I. V. Kumpanenko, K. A. Shiyanova, E. O. Panin, et al., Russ. J. Phys. Chem. B **16**, 1164–1171 (2022). https://doi.org/10.1134/S1990793122060185
23. Y. I. Zuev, M. O. Kostenko, M. Y. Sinev, et al., Russ. J. Phys. Chem. B **17**, 1665–1674 (2023). https://doi.org/10.1134/S1990793123080110
24. L. D. Selezneva, M. V. Podzorova, Y. V. Tertyshnaya, et al., Russ. J. Phys. Chem. B **18**, 555–561 (2024). https://doi.org/10.1134/S1990793124020167
25. F. M. Gumerov, Z. I. Zaripov, S. V. Mazanov, et al., Russ. J. Phys. Chem. B **17**, 1458–1464 (2023). https://doi.org/10.1134/S1990793123070059
26. I. V. Kumpanenko, N. A. Ivanova, N. Y. Kovaleva, et al., Russ. J. Phys. Chem. B **16**, 738–746 (2022). https://doi.org/10.1134/S1990793122040091
27. H. K. Ismail, R. A. Omer, Y. H. Azeez, et al., Synthesis, Russ. J. Phys. Chem. B **18**, 1148–1165 (2024). https://doi.org/10.1134/S1990793124700477
28. T. Chang, F. Fan, Q. Sun, et al., Russ. J. Phys. Chem. B **17**, 680–694 (2023). https://doi.org/10.1134/S1990793123030028
29. L. V. Pavlova, I. A. Platonov, and G. A. Pushkarev, Russ. J. Phys. Chem. B **17**, 1640–1645 (2023). https://doi.org/10.1134/S1990793123080080

30. Y. A. Kurdyaeva, F. S. Bessarab, O. P. Borchevkina, et al., Russ. J. Phys. Chem. B **18**, 852–862 (2024). https://doi.org/10.1134/S1990793124700295
31. N. H. Al-Makishah, M. A. Taleb, and M. A. Barakat, Chem. Pap. **74**, 2743–2757 (2020). https://doi.org/10.1007/s11696-020-01122-4
32. G. Poggere, A. Gasparin, J. Z. Barbosa, et al., J. Trace Elem. Miner. **4**, 100059 (2023). https://doi.org/10.1016/j.jtemin.2023.100059
33. M. Jiang, K. Wang, Y. Wang, et al., Sci. Total Environ. **813**, 151908 (2022). https://doi.org/10.1016/j.scitotenv.2021.151908
34. E. B. da Silva, P. Gao, M.Xu, et al., Environ. Pollut. **264**, 114737 (2010). https://doi.org/10.1016/j.envpol.2020.114737
35. A. D. O.Muñoz, A. Escobedo-Morales, E. Skakerzadeh, et al., J. Mol. Liq. **322**, 114951 (2021). https://doi.org/10.1016/j.molliq.2020.114951
36. D. V. Shtansky, A. T. Matveev, E. S. Permyakova, et al., Nanomaterials **12**, 2810 (2022). https://doi.org/10.3390/nano12162810
37. P. R. Vasyutin, M. Y. Sinev, Y. D. Ivakin, et al., Russ. J. Phys. Chem. B **17**, 1593–1602 (2023). https://doi.org/10.1134/S1990793123080043
38. M. N. Makhov, Russ. J. Phys. Chem. B **18**, 185–188 (2024). https://doi.org/10.1134/S1990793124010147
39. E. A. Yakush, A. V. Kim, and N. N. Medvedev, Russ. J. Phys. Chem. B **18**, 252–257 (2024). https://doi.org/10.1134/S199079312401038X
40. O. N. Fedyaeva, A. P. Grebennikov, and A. A. Vostrikov, Russ. J. Phys. Chem. B **17**, 1628–1639 (2023). https://doi.org/10.1134/S1990793123080079
41. F. Mollaamin and M. Monajjemi, Comput. Theor. Chem. **1237**, 114646 (2024). https://doi.org/10.1016/j.comptc.2024.114646
42. F. Mollaamin and M. Monajjemi, Russ. J. Phys. Chem. B **18**, 1177–1198 (2024). https://doi.org/10.1134/S1990793124700507
43. F. Mollaamin and M. Monajjemi, Russ. J. Phys. Chem. B **18**, 1199–1216 (2024). https://doi.org/10.1134/S1990793124700519
44. J. P. Perdew, K. Burke and M. Ernzerhof, Phys. Rev. Lett. **77**, 3865 (1996). https://doi.org/10.1103/PhysRevLett.77.3865
45. M. A. A. Zadeh, H. Lari, L. Kharghanian, et al., J. Comput. Theor. Nanosci. **12**, 4358 (2015). https://doi.org/10.1166/jctn.2015.4366
46. B. Khalili Hadad, F. Mollaamin, and M. Monajjemi, Russ. Chem. Bull. **60**, 238–241 (2011). https://doi.org/10.1007/s11172-011-0039-5
47. S. H. M. Sheet, R.B.Mahmod, N.H.M. Saeed, et al., New Mater. Compd. Appl. **8**, 94–108 (2024). https://doi.org/10.62476/nmca8194
48. M. Monajjemi, F. Mollaamin, and S. Shojaei, Biointerface Res. Appl. Chem. **10**, 5575 (2020). https://doi.org/10.33263/BRIAC103.575585
49. S. Shahriari, F. Mollaamin, and M. Monajjemi, Micromachines **14**, 241 (2023). https://doi.org/10.3390/mi14020241
50. F. Mollaamin, A. Ilkhani, N. Sakhaei, et al., J. Comput. Theor. Nanosci. **12**, 3148–3154 (2015). https://doi.org/10.1166/jctn.2015.4092
51. M. Monajjemi, L. Mahdavian, F. Mollaamin, et al., Russ. J. Inorg. Chem. **54**, 1465–1473 (2009). https://doi.org/10.1134/S0036023609090216
52. R. Alaya, K. Kourchid, Y. Althaqafi, et al., Russ. J. Phys. Chem. B **17**, 868–877 (2023). https://doi.org/10.1134/S1990793123040024
53. X. Yuan, X. Tan, and B. Liu, Russ. J. Phys. Chem. B **17**, 886–895 (2023). https://doi.org/10.1134/S1990793123040322
54. S. H. Touhami, K. Almi, S. Lakel, et al., Russ. J. Phys. Chem. B **17**, 1057–1068 (2023). https://doi.org/10.1134/S1990793123050287
55. F. Mollaamin and M. Monajjemi, Clean Technol. **5**, 403–417 (2023). https://doi.org/10.3390/cleantechnol5010020
56. F. Mollaamin and M. Monajjemi, J. Comput. Theor. Nanosci. **12**, 1030–1039 (2015). https://doi.org/10.1166/jctn.2015.3846
57. F. Mollaamin and M. Monajjemi, J. Bio Tribo. Corros. **9**, 33 (2023). https://doi.org/10.1007/s40735-023-00751-y
58. F. Mollaamin, M. Monajjemi, S. Salemi, et al., Fullerenes Nanotubes Carbon Nanostruct. **19**, 182 (2011). https://doi.org/10.1080/15363831003782932
59. P. Hohenberg and W. Kohn, Phys. Rev. B **136**, B864–B871 (1964). https://doi.org/10.1103/PhysRev.136.B864
60. W. Kohn and L. J. Sham, Phys. Rev. **140**, A1133–A1138 (1965). https://doi.org/10.1103/PhysRev.140.A1133
61. A. D. Becke, J. Chem. Phys. **98**, 5648–5652 (1993). https://doi.org/10.1063/1.464913
62. C. Lee, W. Yang, and R. G. Parr, Phys. Rev. B **37**, 785–789 (1988). https://doi.org/10.1103/PhysRevB.37.785
63. K. Kim and K. D. Jordan, J. Phys. Chem. **98**, 10089–10094 (1994). https://doi.org/10.1021/j100091a024
64. P. J. Stephens, F. J. Devlin, C. F. Chabalowski, et al., J. Phys. Chem. **98**, 11623–11627 (1994). https://doi.org/10.1021/j100096a001
65. M. Monajjemi, M. Khaleghian, N. Tadayonpour, et al., Int. J. Nanosci. **09**, 517–529 (2010). https://doi.org/10.1142/S0219581X10007071
66. F. Mollaamin and M. Monajjemi, J. Clust. Sci. **34**, 2901–2918 (2023). https://doi.org/10.1007/s10876-023-02436-5
67. F. Mollaamin and M. Monajjemi, J. Mol. Model. **29**, 119 (2023). https://doi.org/10.1007/s00894-023-05526-3
68. M. Monajjemi, F. Mollaamin, S. Shahriari, et al., Russ. J. Phys. Chem. B **18**, 1217–1225 (2024). https://doi.org/10.1134/S1990793124700349
69. F. Mollaamin and M. Monajjemi, C–J. Carbon Res. **9**, 20 (2023).

70. S. Shahriari, M. Monajjemi, and F. Mollaamin, J. Chil. Chem. Soc. **67**, 5468–5476 (2022). https://doi.org/10.4067/S0717-97072022000205468
71. F. Mollaamin and M. Monajjemi, Sens. Rev. **43**, 266–279 (2023). https://doi.org/10.1108/SR-03-2023-0040
72. M. Monajjemi, H. Yamola and F. Mollaamin, Fullerenes Nanotubes Carbon Nanostruct. **22**, 595–603 (2014). https://doi.org/10.1080/1536383X.2012.702163
73. F. Mollaamin, F. Najafi, M. Khaleghian, et al., Fullerenes Nanotubes Carbon Nanostruct. **19**, 653–667 (2011). https://doi.org/10.1080/1536383X.2010.504956
74. M. J. Frisch, G. W. Trucks, H. B. Schlegel, G. E. Scuseria, M. A. Robb, J. R. Cheeseman, G. Scalmani, V. Barone, G. A. Petersson, H. Nakatsuji, X. Li, M. Caricato, A. V. Marenich, J. Bloino, B. G. Janesko, R. Gomperts, B. Mennucci, H. P. Hratchian, J. V. Ortiz, A. F. Izmaylov, J. L. Sonnenberg, D. Williams-Young, F. Ding, F. Lipparini, F. Egidi, J. Goings, B. Peng, A. Petrone, T. Henderson, D. Ranasinghe, V. G. Zakrzewski, J. Gao, N. Rega, G. Zheng, W. Liang, M. Hada, M. Ehara, K. Toyota, R. Fukuda, J. Hasegawa, M. Ishida, T. Nakajima, Y. Honda, O. Kitao, H. Nakai, T. Vreven, K. Throssell, J. A. Montgomery, Jr., J. E. Peralta, F. Ogliaro, M. J. Bearpark, J. J. Heyd, E. N. Brothers, K. N. Kudin, V. N. Staroverov, T. A. Keith, R. Kobayashi, J. Normand, K. Raghavachari, A. P. Rendell, J. C. Burant, S. S. Iyengar, J. Tomasi, M. Cossi, J. M. Millam, M. Klene, C. Adamo, R. Cammi, J. W. Ochterski, R. L. Martin, K. Morokuma, O. Farkas, J. B. Foresman, and D. J. Fox, *Gaussian 16, Revision C.01* (Gaussian, Inc., Wallingford CT, 2016).
75. R. Dennington, T. A. Keith, and J. M. Millam, *GaussView, Version 6.06.16* (Semichem Inc., Shawnee Mission, KS, 2016).
76. F. Mollaamin and M. Monajjemi, Russ. J. Phys. Chem. B **17**, 658–672 (2023). https://doi.org/10.1134/S1990793123030223
77. F. Mollaamin and Monajjemi, M. Russ. J. Phys. Chem. B **18**, 607–623 (2024). https://doi.org/10.1134/S1990793124020271
78. F. Mollaamin, S. Shahriari, and M. Monajjemi, Russ. J. Phys. Chem. B **18**, 398–418 (2024). https://doi.org/10.1134/S199079312402026X
79. F. Mollaamin, Russ. J. Phys. Chem. B **18**, 805–820 (2024). https://doi.org/10.1134/S1990793124700131
80. M. Monajjemi, F. Mollaamin, M. R. Gholami, et al., Main Group Metal Chem. **26**, 349–361 (2003). https://doi.org/10.1515/MGMC.2003.26.6.349
81. M. Monajjemi, A. Sobhanmanesh, and F. Mollaamin, Fullerenes, Nanotubes Carbon Nanostruct. **21**, 47–63 (2013). https://doi.org/10.1080/1536383X.2011.574325
82. F. Mollaamin, Computation **11**, 84 (2023). https://doi.org/10.3390/computation11040084
83. F. Mollaamin, S. Mohammadi, Z.Khalaj, et al., Russ. J. Phys. Chem. B **18**, 67–82 (2024). https://doi.org/10.1134/S1990793124010330
84. F. Mollaamin, S. Shahriari, M. Monajjemi, et al., J. Cluster Sci. **34**, 1547–1562 (2023). https://doi.org/10.1007/s10876-022-02335-1
85. F. Mollaamin and M. Monajjemi, J. Mol. Model. **29**, 170 (2023). https://doi.org/10.1007/s00894-023-05567-8
86. F. Mollaamin, J. Comput. Theor. Nanosci. **11**, 2393–2398 (2014). https://doi.org/10.1166/jctn.2014.3653
87. D. A. Krugovov, A. K. Gatin, N. V. Potapova, et al., Russ. J. Phys. Chem. B **18**, 656–662 (2024). https://doi.org/10.1134/S199079312470012X
88. E. V. Morozov, A. V. Il'ichev, and V. M. Bouznik, Russ. J. Phys. Chem. B **17**, 1361–1369 (2023). https://doi.org/10.1134/S1990793123060064
89. X. Q. Zhang and B. Zhang, Russ. J. Phys. Chem. B **17**, 1049–1056 (2023). https://doi.org/10.1134/S1990793123050135
90. L. I. Trakhtenberg, Russ. J. Phys. Chem. B **17**, 600–607 (2023). https://doi.org/10.1134/S1990793123030144
91. L. K. Abdullayeva and M. H. Hasanov, New Mater. Compd. Appl. **8**, 135–141 (2024). https://doi.org/10.62476/nmca8135
92. Kh. Kh. Hashimov and T. M. Isayeva, New Mater. Compd. Appl. **8**, 121–134 (2024). doi https://doi.org/10.62476/nmca8121
93. A. N. Morozov, S. E. Tabalin, D. R. Anfimov, et al., Russ. J. Phys. Chem. B **18**, 763–772 (2024). https://doi.org/10.1134/S1990793124700234